High frequency forcing on nonlinear systems*

Yao Cheng-Gui(姚成贵)[a], He Zhi-Wei(何志威)[b,c], and Zhan Meng(占 萌)[b,†]

[a] Department of Mathematics, Shaoxing University, Shaoxing 312000, China
[b] Wuhan Center for Magnetic Resonance, State Key Laboratory of Magnetic Resonance and Atomic and Molecular Physics, Wuhan Institute of Physics and Mathematics, Chinese Academy of Sciences, Wuhan 430071, China
[c] University of the Chinese Academy of Sciences, Beijing 100049, China

(Received 6 July 2012; revised manuscript received 24 August 2012)

High-frequency signals are pervasive in many science and engineering fields. In this work, the effect of high-frequency driving on general nonlinear systems is investigated, and an effective equation for slow motion is derived by extending the inertial approximation for the direct separation of fast and slow motions. Based on this theory, a high-frequency force can induce various phase transitions of a system by changing its amplitude and frequency. Numerical simulations on several nonlinear oscillator systems show a very good agreement with the theoretic results. These findings may shed light on our understanding of the dynamics of nonlinear systems subject to a periodic force.

Keywords: high frequency, nonlinear oscillator, inertial approximation, phase transitions

PACS: 05.40.Ca, 87.16.dj **DOI:** 10.1088/1674-1056/22/3/030503

1. Introduction

Nonlinear systems driven by periodic forces can show different kinds of dynamic behavior. One of the best known is frequency locking,[1,2] which indicates that oscillatory systems often adjust their oscillation frequencies to that of external periodic forcing. Some other phenomena have also been extensively observed, such as quasiperiodic oscillations, period doubling, and even chaos in the driven circle maps,[3,4] van der Pol oscillators,[5,6] analog circuits,[7–9] cardiac tissue,[10] and chemical systems.[11] In all those studies, usually a low-frequency forcing, whose frequency is not very far away from the natural frequency of the unforced system, was considered.

On the other hand, in many technical applications, high-frequency signals are pervasive and extremely important. For instance, it is shown that a high-frequency signal can block the conduction in the neural system, which is very useful in many clinical applications.[12–14] A high-frequency stimulation of presynaptic terminals significantly enhances the rate of replenishment of a releasable pool of synaptic vesicles, which is helpful for distinguishing whether presynaptic or postsynaptic mechanisms are responsible for short- and long-term changes of synapses in their strengths in the central nervous system.[15] A high-frequency magnetic force microscope (HF-MFM) can be built for the observation of the high-frequency stray fields of harddisk write heads, which yields HF-MFM images with clearly improved spatial resolution.[16] In the literature, we may find many other important applications for high-frequency signals.

So far, in studies of nonlinear dynamics of oscillation, several classical analytical perturbation methods have been developed,[17–20] such as the Poincare–Lyapunov method of small parameters, the Mathieu method, the asymptotic method, the method of multiple scales, the method of harmonic balance, and the method of direct separation of motions (so-called inertial approximation). Basically, both the Poincare–Lyapunov method of small parameter and the method of multiple scales use the idea of expanding with a small parameter. In the asymptotic method developed by Bogolyubov *et al.*, the solution should first be dealt with the change of variables. The Mathieu method uses the Floquet–Lyapunov's theory for stability analysis of the solutions of systems of linear differential equations with periodic coefficients of any order. In the method of harmonic balance,[21] an infinite set of coupled nonlinear equations is obtained based on the coefficients in front of the different harmonics, and they should be further compared and analyzed. In the inertial approximation analysis, which was first proposed by Blekhman and his co-workers,[17,18] the fast and the slow motions are decomposed and treated separately. The fast motion corresponds to the high-frequency modulation on the slow motion, whose detailed behavior is usually unimportant and can be averaged out over a long time scale. On the contrary, the slow motion behavior is important and determines the essential behavior of the whole system. For forced nonlinear systems with high-frequency excitation, the inertial approximation is quite useful and is believed to have certain advantages over the other methods.[18] For more details about these methods and their comparisons, see Refs. [17]– [20] and references therein.

In the study of forced bistable systems with two different periodic signals, it is found that a weak low-frequency

*Project supported by the National Natural Science Foundation of China (Grant Nos. 11205103 and 11075202).
†Corresponding author. E-mail: zhanmeng@wipm.ac.cn
© 2013 Chinese Physical Society and IOP Publishing Ltd

signal can be enhanced by a high-frequency signal of intermediate amplitude. This phenomenon was first reported by Landa and McClintock in 2000[22] and is termed as the vibrational resonance, which is quite similar to the stochastic resonance for the noise enhanced resonance.[23–27] Since then, the vibrational resonance has been widely investigated in various nonlinear systems, including the excitable model,[28–31] bistable model,[32–39] two coupled overdamped anharmonic oscillators,[40] quintic oscillator,[41,42] and spatially extended systems.[43,44] In addition, Chizhevsky *et al.* provided the first experimental evidence of vibrational resonance in a bistable vertical cavity laser system.[45] In Ref. [46], the inertial approximation[17] has been successfully used to analyze the vibrational resonance, which demonstrated that the addition of high-frequency forcing actually gives rise to the change of the effective stiffness parameter, and thus the resonance appears at the system transition from the bistable behavior to the mono-stable one.

Therefore, it is quite interesting to uncover the peculiar effect of high-frequency signals on nonlinear systems in a general manner. Though the actions of high-frequency perturbations on dynamical systems have been considered in many publications, several different methods have been applied, and a number of generic effects have been derived,[17–20] there is no general theory for high-frequency forcing on nonlinear systems. In addition, we do not know whether the inertial approximation can be extended to this more general case, and the possible interplay between the high-frequency forcing and nonlinear systems remains unclear.

In this work, we investigate the influence of high-frequency forcing on nonlinear oscillator systems, including both periodic and chaotic systems. Based on the analysis of the inertial approximation, we find that the effect of the high-frequency forcing is simple. Due to the changes of the amplitude and the frequency of the high-frequency forcing, the system's dynamic behavior indeed changes and gives rise to various bifurcations. Our analytical results are confirmed by extensive numerical simulations on several different models. We organize this paper as follows. In Section 2, the method of inertial approximation is extended, and a framework for the high-frequency effect is provided. In the following three sections (Sections 3–5), three different types of classical oscillator models are studied and checked, and all results clearly show the validity of the theoretical analysis in Section 2. Finally, we give a summary in Section 6.

2. High-frequency forcing on nonlinear systems

In this section, we generalize the method of inertial approximation,[17] which has been applied to explain the mechanism of vibrational resonance for bistable systems.[46] Here we consider a general forced nonlinear system driven by a high frequency signal

$$\dot{\boldsymbol{x}} = \boldsymbol{f}(\boldsymbol{x}) + \boldsymbol{H}B\cos(\Omega t), \tag{1}$$

where $\boldsymbol{x}(t) \in \mathbf{R}^n$ represents the state vector of the nonlinear system, $\boldsymbol{f}(\boldsymbol{x}) = [f_1(\boldsymbol{x}), f_2(\boldsymbol{x}), \ldots, f_n(\boldsymbol{x})]^{\mathrm{T}}$ stands for a nonlinear function, and $B\cos(\Omega t)$ denotes high frequency forcing with frequency Ω and amplitude B. The unforced system $\dot{\boldsymbol{x}} = \boldsymbol{f}(\boldsymbol{x})$ may exhibit stationary, periodic, or chaotic behavior for different system parameters. Without loss of generality, $\boldsymbol{H} = [1, 1, \ldots 1]^{\mathrm{T}} \in \mathbf{R}^n$, and we only consider the high frequency, namely, Ω should be sufficiently larger than the natural frequency ω of the unforced oscillator system.

By using the method of direct separation of motions,[17,18] the solution $\boldsymbol{x}(t)$ can be decomposed into a slow motion $\boldsymbol{X}(t)$ and a fast motion $\boldsymbol{\Psi}(t)$, i.e.,

$$\boldsymbol{x}(\boldsymbol{t}) = \boldsymbol{X}(\boldsymbol{t}) + \frac{1}{\Omega}\boldsymbol{\Psi}(t, \tau), \tag{2}$$

where $\tau = \Omega t$, $\boldsymbol{X}(t) \in \mathbf{R}^n$, and $\boldsymbol{\Psi} = [\boldsymbol{\Psi}_1, \boldsymbol{\Psi}_2, \ldots, \boldsymbol{\Psi}_n]^{\mathrm{T}} \in \mathbf{R}^n$ is a 2π-periodic function of the fast time $\tau = \Omega t$, with zero mean with respect to this time

$$\overline{\boldsymbol{\Psi}(t, \tau)} = \frac{1}{2\pi}\int_0^{2\pi} \boldsymbol{\Psi}(t, \tau)\,\mathrm{d}\tau = 0. \tag{3}$$

Substituting Eq. (2) into Eq. (1), we obtain

$$\dot{\boldsymbol{X}} + \frac{1}{\Omega}\left(\frac{\partial \boldsymbol{\Psi}}{\partial t} + \Omega\frac{\partial \boldsymbol{\Psi}}{\partial \tau}\right) = \boldsymbol{f}\left(\boldsymbol{X} + \frac{1}{\Omega}\boldsymbol{\Psi}\right) + \boldsymbol{H}B\cos(\Omega t). \tag{4}$$

After using the Taylor series expansion for small values of $\Omega^{-1}(\Omega^{-1} \ll 1)$, we have

$$\begin{aligned}\dot{\boldsymbol{X}} + \frac{1}{\Omega}\frac{\partial \boldsymbol{\Psi}}{\partial t} + \frac{\partial \boldsymbol{\Psi}}{\partial \tau} &= \boldsymbol{f}(\boldsymbol{X}) + \frac{1}{\Omega}\frac{\partial \boldsymbol{f}}{\partial \boldsymbol{X}}\boldsymbol{\Psi} + \frac{1}{2\Omega^2}\boldsymbol{\Psi}^{\mathrm{T}}\frac{\partial^2 \boldsymbol{f}}{\partial \boldsymbol{X}^2}\boldsymbol{\Psi} \\ &\quad + \boldsymbol{H}B\cos(\tau) + \boldsymbol{C},\end{aligned} \tag{5}$$

where $\partial \boldsymbol{f}/(\partial \boldsymbol{X})$ is the Jacobian matrix,

$$\begin{aligned}\boldsymbol{\Psi}^{\mathrm{T}}\frac{\partial^2 \boldsymbol{f}}{\partial \boldsymbol{X}^2}\boldsymbol{\Psi} &= \left[\boldsymbol{\Psi}^{\mathrm{T}}\frac{\partial^2 f_1}{\partial \boldsymbol{X}^2}\boldsymbol{\Psi}, \boldsymbol{\Psi}^{\mathrm{T}}\frac{\partial^2 f_2}{\partial \boldsymbol{X}^2}\boldsymbol{\Psi}, \ldots, \boldsymbol{\Psi}^{\mathrm{T}}\frac{\partial^2 f_n}{\partial \boldsymbol{X}^2}\boldsymbol{\Psi}\right]^{\mathrm{T}} \\ &= \Big[\sum_{i,j=1}^{n}\frac{\partial^2 f_1}{\partial X_i \partial X_j}\Psi_i\Psi_j, \sum_{i,j=1}^{n}\frac{\partial^2 f_2}{\partial X_i \partial X_j}\Psi_i\Psi_j, \ldots, \\ &\quad \sum_{i,j=1}^{n}\frac{\partial^2 f_n}{\partial X_i \partial X_j}\Psi_i\Psi_j\Big]^{\mathrm{T}},\end{aligned}$$

and $\boldsymbol{C}$ represents high-order Taylor terms.

Under the hypothetic condition for slow and fast motions, we obtain the following evolution equations for $\boldsymbol{X}(t)$ and $\boldsymbol{\Psi}(t)$:

$$\dot{\boldsymbol{X}} = \boldsymbol{f}(\boldsymbol{X}) + \frac{1}{2\Omega^2}\overline{\boldsymbol{\Psi}^{\mathrm{T}}\frac{\partial^2 \boldsymbol{f}}{\partial \boldsymbol{X}^2}\boldsymbol{\Psi}}, \tag{6a}$$

$$\begin{aligned}\frac{\partial \boldsymbol{\Psi}}{\partial \tau} &= \frac{1}{\Omega}\left[-\frac{\partial \boldsymbol{\Psi}}{\partial t} + \frac{\partial \boldsymbol{f}}{\partial \boldsymbol{X}}\boldsymbol{\Psi} + \frac{1}{2\Omega}\left(\boldsymbol{\Psi}^{\mathrm{T}}\frac{\partial^2 \boldsymbol{f}}{\partial \boldsymbol{X}^2}\boldsymbol{\Psi} - \overline{\boldsymbol{\Psi}^{\mathrm{T}}\frac{\partial^2 \boldsymbol{f}}{\partial \boldsymbol{X}^2}\boldsymbol{\Psi}}\right)\right] \\ &\quad + \boldsymbol{H}B\cos(\tau),\end{aligned} \tag{6b}$$

where the overbar denotes the time integral within a period T ($T = 2\pi/\Omega$), and the high-order Taylor terms $\boldsymbol{C}$ have been ne-

glected. The approximate equation for the fast motion $\boldsymbol{\Psi}$ can be obtained by the first-order approximation of Eq. (6b)

$$\frac{\partial \boldsymbol{\Psi}}{\partial \tau} = \boldsymbol{H} B \cos(\tau). \tag{7}$$

We then have

$$\boldsymbol{\Psi}(t,\tau) = \boldsymbol{H} B \sin(\tau) + \boldsymbol{A}(t), \tag{8}$$

where $\boldsymbol{A}(t) = 0$ due to $\overline{\boldsymbol{\Psi}(t,\tau)} = 0$, so $\boldsymbol{\Psi} = \boldsymbol{H} B \sin(\Omega t)$.

By taking into account that

$$\overline{\boldsymbol{\Psi}^{\mathrm{T}} \frac{\partial^2 \boldsymbol{f}}{\partial \boldsymbol{X}^2} \boldsymbol{\Psi}} = \frac{B^2}{2} \boldsymbol{H}^{\mathrm{T}} \frac{\partial^2 \boldsymbol{f}}{\partial \boldsymbol{X}^2} \boldsymbol{H},$$

the equation for the slow motion $\boldsymbol{X}(t)$ from Eq. (6a) becomes

$$\dot{\boldsymbol{X}} = \boldsymbol{f}(\boldsymbol{X}) + \frac{D}{4} \boldsymbol{H}^{\mathrm{T}} \frac{\partial^2 \boldsymbol{f}}{\partial \boldsymbol{X}^2} \boldsymbol{H}, \tag{9}$$

where $D = B^2/\Omega^2$. Comparing this equation for the slow motion $\boldsymbol{X}(t)$ with Eq. (1) for the whole forced system $\boldsymbol{x}(t)$, we can clearly find that the old right driving term becomes more specific (without dependence on time now) and the effect of high-frequency forcing becomes apparent. From the mathematical point of view, the non-autonomous equation (Eq. (1)) has become autonomous, and the system dimension decreases as the equation for fast motion has been dropped completely. Clearly, now the information of the high-frequency signal (including both the intensity B and the frequency Ω) has directly come into the system's evolution equation, and thus the value of D (combining B and Ω) will determine the dynamic behavior of the slow motion in Eq. (9) and further determine that of the whole forced system in Eq. (1). Note that for different forms of $\boldsymbol{H}$, though the effective equation might be different from Eq. (9), this simple physical picture might be unchanged.

Here it is necessary to discuss the general equation in Eq. (9) with other classical approximation methods. Clearly, the Poincare–Lyapunov method and the Mathieu method of using the Floquet–Lyapunov's theory cannot give an explicit form for the slow motion. For the method of multiple scales, the equation is also not available, as we consider a general nonlinear function here. By using the asymptotic method, surprisingly, a slightly different equation is obtained, however its accuracy is not guaranteed. For the method of harmonic balance, after a long comparison for the harmonic terms and algebra manipulation, exactly the same equation as Eq. (9) can be obtained. Thus, compared to all other methods, we can clearly see the method of direct separation of motions has a physical clearness and is easy to handle, especially in dealing with the current problem.

Below we will give three examples to check the validity of this theory.

3. Periodic system I

As the first example, the Landau–Stuart periodic system,[1] which is the normal form of the Hopf bifurcation, is considered

$$\dot{Z} = (a + \mathrm{i}\omega - |Z|^2) Z, \tag{10}$$

where Z is a complex number, a signals a parameter specifying the distance from the Hopf bifurcation, and ω denotes the intrinsic frequency of the system. It can also be rewritten in the polar coordinates as

$$\dot{r} = (a - r^2) r, \ \ \dot{\theta} = \omega. \tag{11}$$

The dynamics of the Landau–Stuart system is well known.[1] If $a < 0$, a steady state staying at the origin is stable, whereas if $a > 0$, this steady state loses its stability, and the system generates a new stable limit cycle, whose rotation semi-diameter is $\sqrt{a}$ and rotation frequency is ω. This bifurcation is a supercritical Hopf bifurcation, and $a = 0$ is usually called the Hopf bifurcation point. Without loss of generality, we set $a = 1$ in the above standard equation. Therefore, the unforced system is oscillatory, which has an unstable focus at the origin ($Z = 0$) and an attracting limit cycle $Z(t) = \mathrm{e}^{\mathrm{i}\omega t} = x(t) + \mathrm{i}y(t)$.

Furthermore, the dynamics of this system driven by a high-frequency signal can be described in the Cartesian coordinates as

$$\dot{x} = (1 - x^2 - y^2)x - \omega y + B\cos(\Omega t), \tag{12a}$$

$$\dot{y} = (1 - x^2 - y^2)y + \omega x + B\cos(\Omega t), \tag{12b}$$

where $B\cos(\Omega t)$ is a high frequency force. Without loss of generality, $\omega = 0.1$ is always chosen, and thus the condition of a sufficiently large Ω ($\Omega \gg \omega$) is maintained.

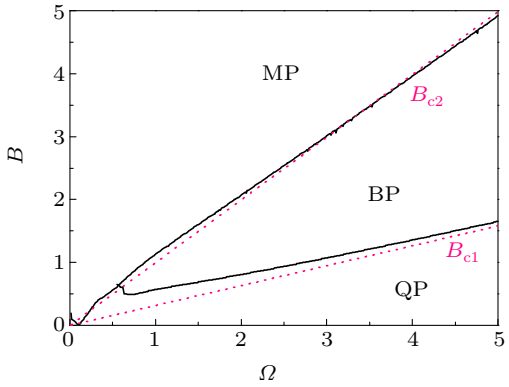


Fig. 1. (color online) Phase diagram on the (Ω, B) plane for different dynamic parameters of the forced Landau–Stuart oscillator (Eq. (12)). The two straight dashed critical lines B_{c1} and B_{c2} come from the analyses in Eqs. (17) and (16), respectively.

The phase diagram of the system on plane (Ω, B) is shown in Fig. 1 based on the integration of the above equations. Three different types of dynamic regions: quasiperiod (QP), bistable period (BP), and mono-stable period (MP), are clear. The quasiperiodic region is characterized by two zero Lyapunov exponents $\lambda_1 = 0$ and $\lambda_2 = 0$. All periodic regions including BP and MP are characterized by only one zero Lyapunov exponent $\lambda_1 = 0$, and $\lambda_2 < 0$. The critical curve for the transition from monostable periodic state to bistable periodic

state is determined by the change from the monostable behavior to the bistable one. Two critical (dashed) curves B_{c1} and B_{c2} from the theory, which are linearly dependent on Ω, are also superimposed; see below for more details.

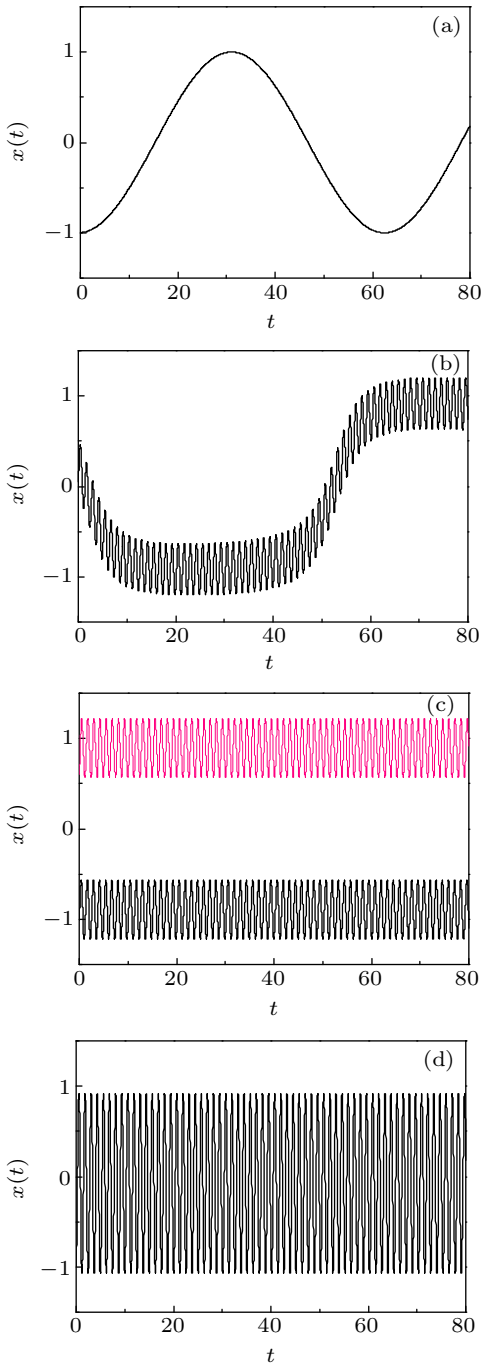


Fig. 2. (color online) The time series of $x(t)$ for (a) $B = 0.0$, (b) $B = 1.5$, (c) $B = 1.7$, and (d) $B = 5.0$, where $\Omega = 5.0$. In panel (c), the bistable behavior is clearly shown by using two different colors for different initial conditions.

To make it clear, we show the detailed time series of $x(t)$ in Figs. 2(a)–2(d) for $B = 0$, $B = 1.5$, $B = 1.7$, and $B = 5.0$, respectively; and $\Omega = 5.0$. For $B = 0$, the sinusoidal curve is clear (Fig. 2(a)). For $B = 1.5 < B_{c1} = 1.65$ in the region of QP, $x(t)$ shows a quasiperiodic motion constituted with two different components: the fast high-frequency Ω and the slow basal part (Fig. 2(b)). For $B = 1.7$ in BP, $x(t)$ becomes fluctuating periodically around different finite values for different initial conditions (Fig. 2(c)). In this panel, we use different color lines to show this effect. For a sufficiently large B, $x(t)$ can only oscillate rapidly around 0, and the monostable behavior is obvious, as shown in Fig. 2(d). All these time series clearly exemplify the changes of dynamical behaviors for different values of Ω and B.

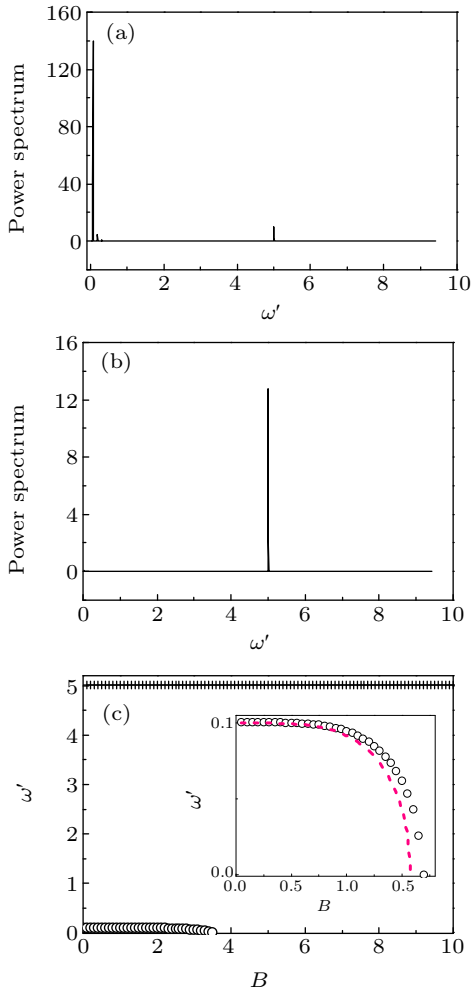


Fig. 3. (color online) The power spectra of $x(t)$ for (a) $B = 1.5$ and (b) $B = 1.7$, where $\Omega = 5.0$. (c) The peak frequency ω' in the power spectrum of $x(t)$ versus B, which shows a clear change of two-value to single-value at B_{c1} ($B_{c1} \approx 1.65$). The inset shows the enlarged part of the left bottom of panel (c). The dashed line comes from the theoretical prediction $\omega' = \sqrt{\omega^2 - D^2}$, where $D = B^2/\Omega^2$.

The underlying mechanism for the phase transition from QP to BP may be well understood based on the frequency analysis. Figures 3(a) and 3(b) show the power spectra of $x(t)$ for $B = 1.5$ (in QP) and $B = 1.7$ (in BP), respectively. Observing these two figures, we find that the same high-frequency component ($\omega' = \Omega = 5.0$) persists, as the system is always driven by the high-frequency signal Ω. However, we do find that a low-frequency component at ω' [$\omega' \approx 0.067$ in Fig. 3(a)] disappears when B is above threshold B_{c1}. To be clear, we plot these frequency peaks for different B's in Fig. 3(c) and

its enlargement in the inset. A transition from two-values to a single-value at $B_{c1} \approx 1.65$ is obvious.

We now apply the theoretical result in Eq. (9) to analyze this system. From Eq. (12), we immediately have

$$\boldsymbol{f} = [f_1, f_2]^{\mathrm{T}} = [x(1-x^2-y^2) - \omega y, y(1-x^2-y^2) + \omega x]^{\mathrm{T}},$$

so

$$\begin{aligned} \boldsymbol{H}^{\mathrm{T}} \frac{\partial^2 \boldsymbol{f}}{\partial X^2} \boldsymbol{H} &= \left[\boldsymbol{H}^{\mathrm{T}} \frac{\partial^2 f_1}{\partial X^2} \boldsymbol{H}, \boldsymbol{H}^{\mathrm{T}} \frac{\partial^2 f_2}{\partial X^2} \boldsymbol{H} \right] \\ &= [-8X - 4Y, -4X - 8Y]^{\mathrm{T}}. \end{aligned}$$

According to Eq. (9), the slow motion should be determined by

$$\dot{X} = (1 - X^2 - Y^2)X - \omega Y - (2X + Y)\frac{B^2}{\Omega^2}, \quad (13a)$$

$$\dot{Y} = (1 - X^2 - Y^2)Y + \omega X - (X + 2Y)\frac{B^2}{\Omega^2}, \quad (13b)$$

which, for convenience, can be rewritten in a compact form as

$$\dot{X} = (1 - X^2 - Y^2 - 2D)X - (\omega + D)Y, \quad (14a)$$

$$\dot{Y} = (1 - X^2 - Y^2 - 2D)Y + (\omega - D)X, \quad (14b)$$

where $D = B^2/\Omega^2$.

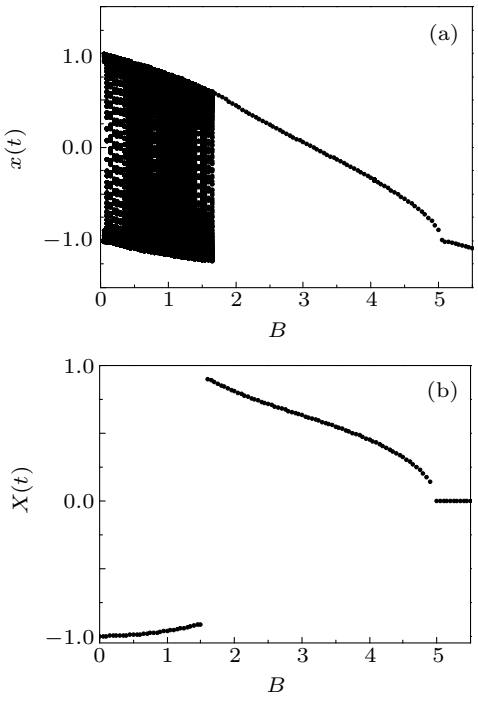


Fig. 4. Bifurcation diagrams of (a) $x(t)$ (Eq. (12)) and (b) $X(t)$ (Eq. (14)), showing two system bifurcations subsequently at $B_{c1} \approx 1.65$ and $B_{c2} \approx 5.0$.

For an immediate comparison, figures 4(a) and 4(b) show the bifurcation diagrams of $x(t)$ and $X(t)$, respectively, for the local minimal values. The initial conditions with positive values are chosen arbitrarily. The top figure for $x(t)$ stands for the numerical result from the direct integration of the driven system (Eqs. (12a) and (12b)), and the bottom one for $X(t)$ is from the inertial approximation theory (Eqs. (14a) and (14b)). Though the specific values of $x(t)$ and $X(t)$ in the bifurcation diagrams are different, they qualitatively exhibit the same values for the two transitions: the first one from QP to BP occurs at $B_{c1} \approx 1.65$, and the second one from BP to MP at $B_{c2} \approx 5.0$.

By analyzing the fixed points and their stabilities in the simplified equation (Eqs. (14a) and (14b)) for the slow motion only, we can easily obtain more system information. For instance, for the fixed point at origin ($X_0 = 0$, $Y_0 = 0$), its stability is determined by the eigenvalue of the linearization equation

$$\lambda_0 = 1 - 2D \pm \sqrt{D^2 - \omega^2}. \quad (15)$$

We show the values of X_0 and Y_0 in Figs. 5(a) and 5(b), respectively, and the corresponding stability analysis for the maximal eigenvalue λ_0 in Fig. 5(c). The other four fixed points are also plotted. In the figures, we use sold lines for stable fixed points and dashed lines for unstable ones, which are determined by their corresponding eigenvalues $\lambda < 0$ and $\lambda > 0$, respectively.

In Fig. 5(c), it shows that the origin is stable if $B > B_{c2}$. The value of B_{c2} can be determined by the condition of $\lambda_0 = 0$ to be

$$B_{c2} = \Omega \sqrt{\frac{2 + \sqrt{1 - 3\omega^2}}{3}}. \quad (16)$$

As B decreases, λ_0 becomes complex if $D < \omega$, and a pair of complex conjugate eigenvalues appear after $B < B_{c1}$. From Eq. (15), we have

$$B_{c1} = \Omega \sqrt{\omega}. \quad (17)$$

In addition, based on the theory of Hopf bifurcation, a limit cycle with the frequency

$$\omega' = \sqrt{\omega^2 - \frac{B^4}{\Omega^4}} \quad (18)$$

might be formed.

From Eqs. (16) and (17), clearly both B_{c1} and B_{c2} linearly depend on Ω. As $\omega = 0.1 \ll 1$, $B_{c1} \approx 0.32\Omega$ and $B_{c2} \approx \Omega$; these two straight lines from the theory have been added in Fig. 1, showing a clear fit with the numerical result. For the specific value of $\Omega = 5.0$, we have $B_{c1} \approx 1.58$ and $B_{c2} \approx 5.0$; these two critical values can be well obtained from the bifurcation diagrams for $x(t)$ and $X(t)$ in Fig. 4. Apart from these, the prediction of Eq. (18) has been well proven with the plot of the dashed line in the inset of Fig. 3(c).

The other nonzero fixed points of Eqs. (14a) and (14b) and their stabilities can also be numerically solved and analyzed. The results are illustrated in Fig. 5. Based on these results, we can observe that only an unstable ($X = 0$, $Y = 0$) exists for $B < B_{c1}$, and all four nonzero real roots (X_1, Y_1), (X_2, Y_2), (X_3, Y_3), (X_4, Y_4) appear only for $B > B_{c1}$. The two fixed points (X_1, Y_1) and (X_2, Y_2) are stable at $B_{c2} > B > B_{c1}$, and they become complex for $B > B_{c2}$. The other two fixed points (X_3, Y_3) and (X_4, Y_4) are always unstable at $B_{c3} > B > B_{c1}$, and do not exist after $B > B_{c3}$, where $B_{c3} \approx 2.91$. There-

fore, at $B_{c2} > B > B_{c1}$, only two fixed points (X_1, Y_1) and (X_2, Y_2) are significant and might contribute to the slow motion.

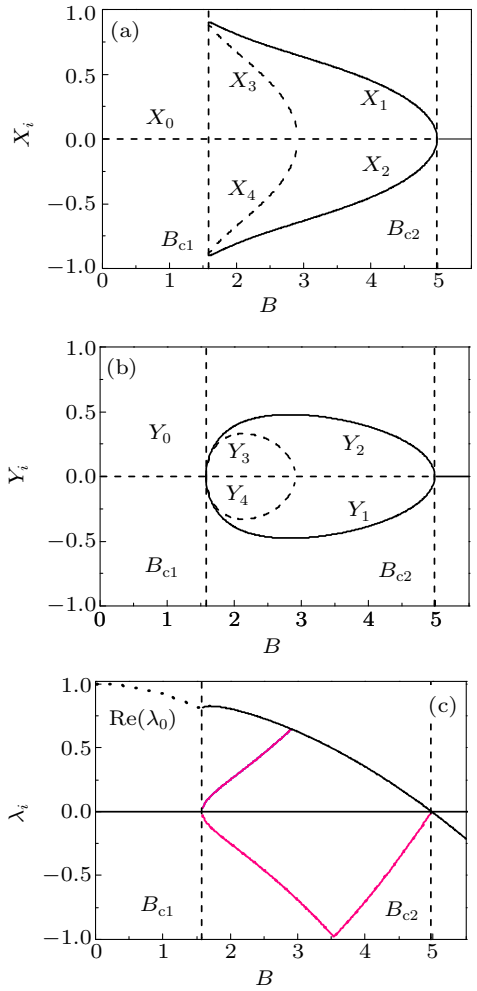


Fig. 5. (color online) Dynamic analysis of the fixed points (a) X_i and (b) Y_i $(i = 0, 1, 2, 3, 4)$ of slow motion. The solid (dashed) lines stand for stable (unstable) fixed points. (c) The corresponding maximal eigenvalues λ_i for all fixed points X_i and Y_i. The dotted line stands for the real part of λ_0, as λ_0 becomes complex if $B < B_{c1}$.

Based on the above observations, with the decreased order of B, the origin loses its stability at $B = B_{c2}$, and meanwhile two new stable fixed points (X_1, Y_1) and (X_2, Y_2) are formed. Thus, a supercritical pitchfork bifurcation occurs, which causes the original driven system to transit from a monostable periodic state to a bistable periodic state. With decreasing B, a pair of complex conjugate eigenvalues of (X_0, Y_0) emerge at B_{c1}, and simultaneously two stable fixed points (X_1, Y_1), (X_2, Y_2) and two unstable fixed points (X_3, Y_3), (X_4, Y_4) collide and disappear. Therefore, a Hopf bifurcation and a saddle-node bifurcation take place simultaneously at B_{c1}, indicating a jump of the original driven system from the bistable periodic state to the quasiperiodic state. As we have seen above, all these analytical results from the inertial approximation have been confirmed by the direct numerical results.

4. Periodic system II

In order to gain more insight into the role of a high-frequency signal on periodic systems and understand the efficiency of the method of inertial approximation, we analyze another two-dimensional periodic oscillator, which is generated by the saddle-node bifurcation on a loop (or the so-called infinite-period bifurcation)[1]

$$\dot{r} = (1 - r^2)r, \quad \dot{\theta} = b - r^2\cos(2\theta), \tag{19}$$

where b is the control parameter. Clearly this system combines two one-dimensional systems. For $b > 1$, the system has a stable limit cycle with $r = 1$ and frequency ω $(\omega = 1/\int_0^{2\pi} \mathrm{d}\theta/(b - \cos(2\theta)))$. The limit cycle disappears via saddle-node bifurcation on the loop at $b = b_c = 1$. For $b < 1$, we have four fixed points on the circle $r = 1$ with $\theta = \pm \arccos b/2$. Two of these fixed points are stable, and the other two are unstable. The stable and the unstable fixed points approach each other as b approaches 1, and they collide at $b = b_c = 1$ and disappear for $b > 1$. Due to its simplicity, this model has been the subject of many earlier studies, such as in the framework of stochastic resonance without an external periodic force.[47,48]

In the Cartesian coordinates, the model subject to a high-frequency signal can be expressed as

$$\dot{x} = (1 - x^2 - y^2)x + (x^2 - y^2 - b)y + B\cos(\Omega t), \tag{20a}$$

$$\dot{y} = (1 - x^2 - y^2)y - (x^2 - y^2 - b)x + B\cos(\Omega t), \tag{20b}$$

where parameter $b = 1.01$ has been chosen with the corresponding frequency $\omega \approx 0.14$.

Figure 6 shows the phase diagram on plane (Ω, B). There are three well-divided regions: the quasiperiodic region, the bistable periodic region, and the monostable periodic region. It is notable that the MP now only exists for small Ω. For large Ω, QP and BP exist, with only one type of transition. As we will see below, this critical behavior is also revealed by our theory.

The time series of $x(t)$ are shown in Figs. 7(a)–7(c) for the parameters within these three different regions. In Fig. 7(a), $\Omega = 5.0$ and $B = 0.4$ in the QP region, in Fig. 7(b), $\Omega = 5.0$ and $B = 0.6$ in the BP region, and in Fig. 7(c), $\Omega = 0.04$ and $B = 0.3$ in the MP region. For the high frequency forcing ($\Omega = 5.0$), if $B < B_c$ ($B_c = 0.5$), $x(t)$ oscillates quasiperiodically (Fig. 7(a)). Conversely, if $B > B_c$ (Fig. 7(b)), $x(t)$ shows bistable periodic behavior, i.e., for different initial conditions, different asymptotic behaviors are possible, as shown by the different color lines in the figure. Additionally, the monostable periodic state only appears at small frequency forcing (Fig. 7(c)).

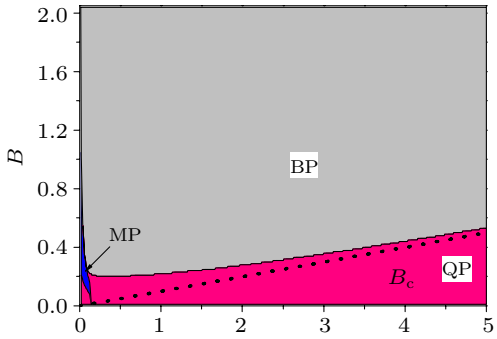


Fig. 6. (color online) Schematic phase diagram of dynamics in Eq. (20) on the (Ω, B) plane. Three different regions correspond to quasiperiodic, bistable periodic, and monostable periodic states, respectively. The black dotted line B_c (Eq. (23)) comes from the analysis.

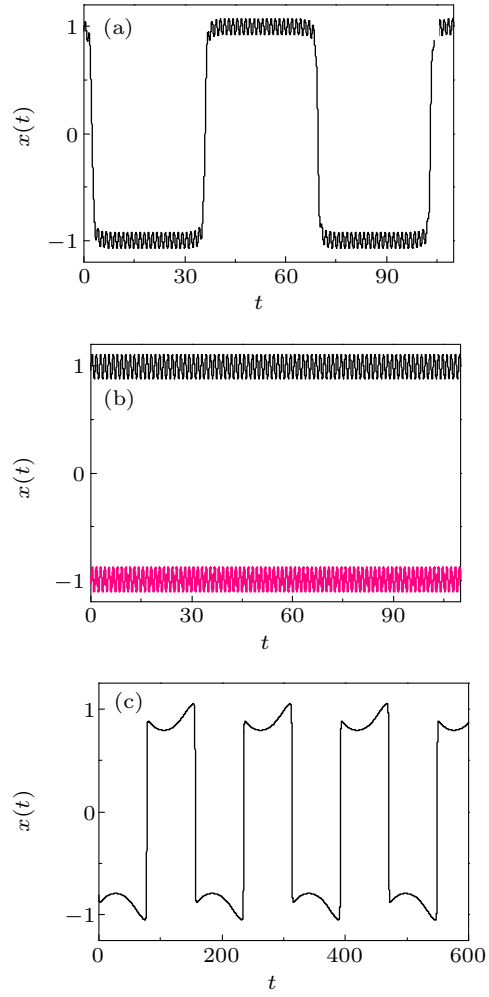


Fig. 7. (color online) The time series of $x(t)$ for three different parameter sets: (a) $\Omega = 5.0$, $B = 0.4$; (b) $\Omega = 5.0$, $B = 0.6$; and (c) $\Omega = 0.04$, $B = 0.3$. For the bistable periodic behavior, we use different colors for the different initial conditions in panel (b).

We may directly apply the theory of inertial approximation (Eq. (9)) to this case and have

$$\dot{X} = (1 - D - X^2 - Y^2)X + Y(X^2 - Y^2 - b - 2D), \quad (21a)$$

$$\dot{Y} = (1 - D - X^2 - Y^2)Y - X(X^2 - Y^2 - b + 2D), \quad (21b)$$

where $D = B^2/\Omega^2$. The comparison of the bifurcation diagrams of $x(t)$ and $X(t)$ is given in Fig. 8. Clearly in the top panel, the phase transition of $x(t)$ from quasiperiodic to periodic takes place at $B_c \approx 0.5$. While at the same B, a jump of $X(t)$ from the periodic state to the stationary state is obvious in the bottom panel.

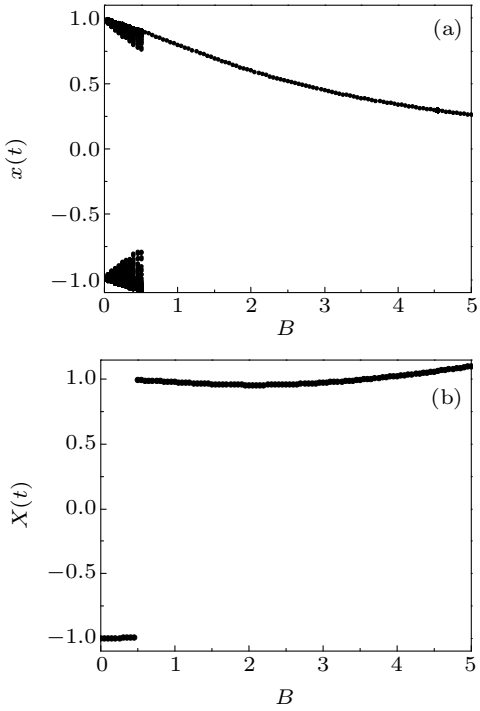


Fig. 8. Bifurcation diagrams of (a) $x(t)$ (Eq. (20)) and (b) $X(t)$ (Eq. (21)), indicating a phase transition at $B_c \approx 0.5$.

Similarly, we can numerically analyze the fixed points of $X(t)$ with Eqs. (21a) and (21b) and their stabilities with the linearization equation. The results are shown in Fig. 9. We can find that (i) there are two stable nonzero fixed points (X_2, Y_2) and (X_3, Y_3) and two unstable nonzero fixed points (X_1, Y_1) and (X_4, Y_4) if $B \geq B_c$; (ii) these four fixed points collide and disappear at B_c, indicating a saddle-node bifurcation for the appearance of phase transition from the bistable periodic state to the quasiperidic state; (iii) the unstable fixed points (X_1, Y_1) and (X_4, Y_4) disappear at a larger B ($B \approx 3.75$).

From Fig. 9(a), we can find that $X_i \neq 0$ and $Y_i = 0$ $(i = 1, 2, 3, 4)$ at B_c. Hence we have

$$1 - D - X^2 = 0, \quad (22a)$$

$$X^2 - b + 2D = 0. \quad (22b)$$

Therefore, $1 - D = 2D - b$, and the condition for the critical value B_c of the saddle-node bifurcation can be derived as

$$B_c = \sqrt{b - 1}\Omega, \quad (23)$$

which again shows that B_c linearly depends on Ω. This linear relationship is plotted with a dashed line in Fig. 6. For $\Omega = 5.0$, $B_c = 0.5$, which perfectly matches our numerical result.

Finally, the stability for the origin fixed point $(X_0 = 0, Y_0 = 0)$ can also be analyzed, and the eigenvalue of the lin-

eailzation equation is expressed as

$$\lambda_0 = 1 - D \pm \sqrt{4D^2 - 2b^2}. \tag{24}$$

The result in Fig. 9 shows that the origin is always unstable in the B parameter region of interest, which may have no significant contribution to the system bifurcation, as we have seen before.

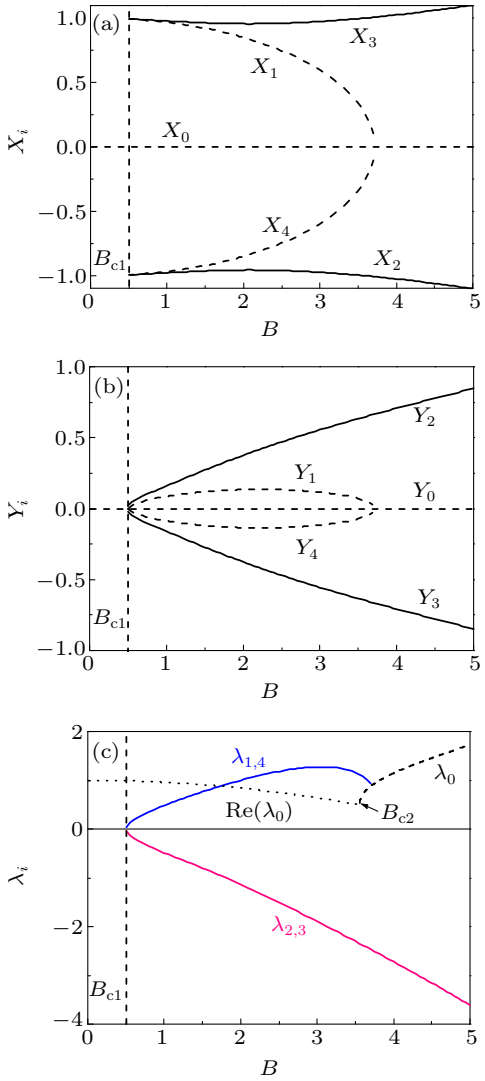


Fig. 9. (color online) Dynamic analysis of the fixed points (a) X_i and (b) Y_i ($i = 0, 1, 2, 3, 4$) of slow motion in Eq. (21). The solid (dashed) lines stand for stable (unstable) fixed points. (c) The maximal eigenvalues λ_i versus B.

5. Chaotic Duffing system

As the third example, we consider the chaotic Duffing oscillator[1] driven by biharmonic signals with two very different frequencies

$$\ddot{x} + \delta\dot{x} - x + x^3 = \gamma\cos(\omega t) + B\cos(\Omega t + \phi), \tag{25}$$

where δ is the damping coefficient, $\gamma\cos(\omega t)$ indicates a low-frequency signal, and $B\cos(\Omega t + \phi)$ stands for a high-frequency signal. Again without loss of generality, $\Omega \gg \omega$. In this situation, the value of the phase angle ϕ is unimportant. Nevertheless, if Ω and ω are comparable, ϕ should be important in determining the system's dynamic behavior; this phase control method[49,50] was first proposed and experimentally demonstrated by Meucci *et al.* In the absence of a high-frequency signal, i.e., $B = 0$, the system is capable of exhibiting chaotic or periodic motion for different system parameters. In our study, the parameter set $\delta = 0.3$, $\gamma = 0.5$, $\omega = 0.41$, and $\phi = 0$ is always chosen, at which the oscillator is chaotic.

Figure 10 shows the schematic phase diagram for different dynamic behaviors. They are determined by the sign of the maximal Lyapunov exponent λ_1, namely, the system is chaotic (gray region) if $\lambda_1 > 0$, while periodic (white region) if $\lambda_1 = 0$. From this figure, we find that even within the periodic region, chaos is available for small Ω, and on the other hand, periodicity can be observed within the chaotic region for certain Ω and B. However, to our surprise, the whole parameter region is well separated by a critical line B_c for the two opposite dynamic behaviors (chaotic and periodic).

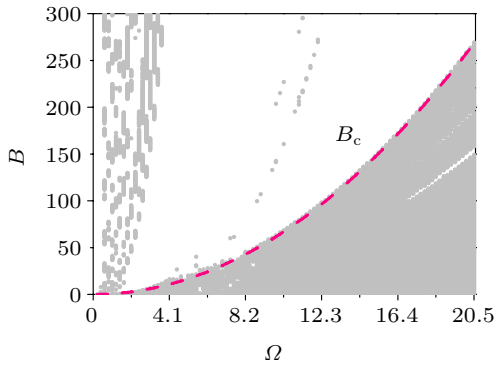


Fig. 10. (color online) Schematic phase diagram for the forced Duffing oscillator in Eq. (25), showing two different dynamic behaviors: the chaotic state within the white region and the periodic state within the gray region. The dashed line B_c superimposed for the division comes from the prediction in Eq. (28).

Figure 11(a) plots all three Lyapunov exponents (λ_i) of the system each as a function of B, where $\Omega = 40\omega = 16.4$. From this figure, we can easily observe that the periodic behavior ($\lambda_1 = 0$) is scattered within the chaotic region at $B < B_c$, and the system is periodic in a pure manner for $B > B_c$ and large Ω. Thus, a critical value B_c exists, indicating that the chaos can be inhibited and controlled by a sufficiently large high-frequency driving. To proceed further, the time series of $x(t)$ are shown in Figs. 12(a)–12(d) for $B = 5$, 23, 100, and 200, respectively, where $\Omega = 40\omega = 16.4$ is unchanged. In Figs. 12(a) and 12(c), the system is chaotic, whereas in Figs. 12(b) and 12(d), the system is periodic.

The Duffing oscillator subject to biharmonical signals has been investigated in the context of vibrational resonance by the method of inertial approximation.[18,32] Here we give an explicit expression for the slow motion. Though now $H \neq [1, 1, \ldots, 1]^{\mathrm{T}}$, following the same basic idea of the inertial approximation, we can decompose $x(t)$ into a slow motion $X(t)$ and a fast motion $\Psi(t)$ of frequency Ω, and further have the

evolution equation of the slow motion $X(t)$

$$\ddot{X} + \delta\dot{X} - \left(1 - \frac{3B^2}{2\Omega^4}\right)X + X^3 = \gamma\cos(\omega t), \tag{26}$$

which, for convenience, can be rewritten as

$$\ddot{X} + \delta\dot{X} - aX + X^3 = \gamma\cos(\omega t), \tag{27}$$

where $a = 1 - 3B^2/(2\Omega^4)$. Therefore, the pure effect of the high-frequency signal in the forced Duffing oscillator is to change the system parameter of the potential.

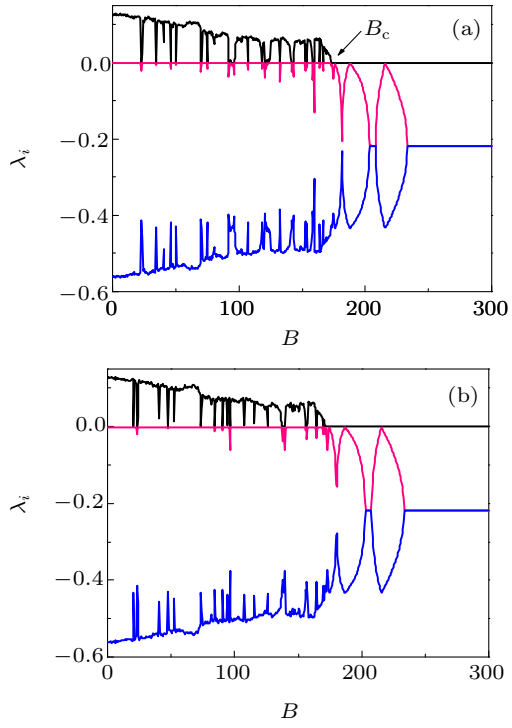


Fig. 11. (color online) (a) The three Lyapunov exponents λ_i of the driven system (Eq. (25)) and (b) those of the system of slow motion (Eq. (26)). A critical B_c exists, which signals a jump from chaotic (still scattered by many periodic windows) to periodic.

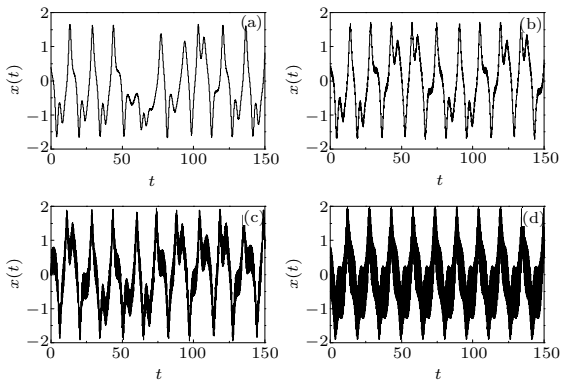


Fig. 12. The time series of $x(t)$ for (a) $B = 5$, (b) $B = 23$, (c) $B = 100$, and (d) $B = 200$, showing different dynamics of the high-frequency signal on the chaotic Duffing oscillator, where $\Omega = 16.4$.

The Lyapunov exponent spectrum (λ_i) of Eq. (26) is also calculated for different B's. The result is shown in Fig. 11(b). Comparing these two figures (the original forced system $x(t)$ in Fig. 11(a) and the reduced system $X(t)$ of the slow motion in Fig. 11(b)), we find that they are nearly the same.

In order to estimate the critical value B_c, the Lyapunov exponents (λ_i) of Eq. (27) for different a are computed, as shown in Fig. 13(a), and the corresponding bifurcation diagram is shown in Fig. 13(b). From these figures, a clear critical value a_c ($a_c \approx 0.39$) is observed, indicating the system transition from periodic to chaotic. Based on this value, B_c can be estimated as

$$B_c = \Omega^2\sqrt{2(1-a_c)/3} \approx 0.638\Omega^2. \tag{28}$$

This quadratic relationship between B_c and Ω has been perfectly verified by the numerical result, as shown by the dashed curve in Fig. 10.

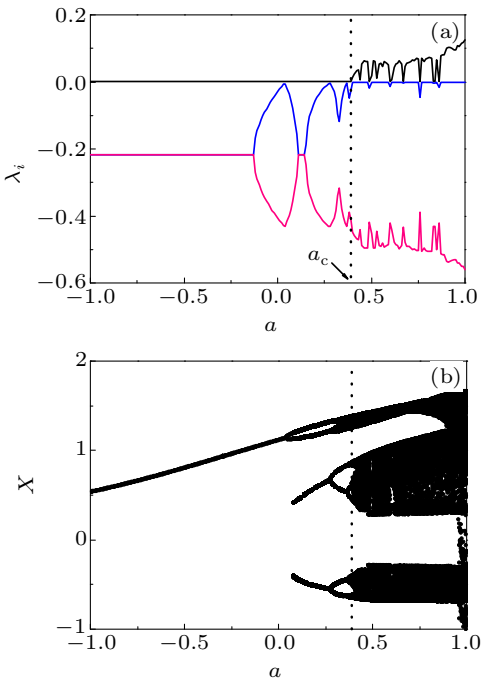


Fig. 13. (color online) (a) The Lyapunov exponents λ_i and (b) the bifurcation diagram of $X(t)$ each as a function of a, showing a critical a_c ($a_c \approx 0.39$). Based on this value, the quantitative relationship between B_c and Ω in Fig. 10 is well determined.

Finally, it is noticed that the chaotic Duffing oscillator driven by bi-harmonic signals with two very different frequencies was analytically and numerically studied previously by Kivshar *et al.*[21] in the context of chaos suppression. There, the method of harmonic balance was used. Though the specific term for the added high-frequency signal in Ref. [21] is different to ours in Eq. (25), we may also apply the harmonic balance method for our problem and finally get the same result shown in Eq. (26). This indicates that with different approximation methods, the finial form of the effective and averaged equation for the slowly varying component of the oscillation amplitude might be the same. This also indicates that the inertial approximation for the direct separation of fast and slow motions is correct.

6. Summary

We have made a detailed study on the role of high-frequency force on different types of nonlinear oscillatory systems. A general equation based on theoretical analysis with the inertial approximation, which directly separates fast and slow motion, has been derived. The same equation can also be obtained by using the method of harmonic balance. Extensive numerical results show that the high-frequency signal with a sufficiently strong intensity can actually induce various bifurcations, which can actually be analyzed by using the simplified theoretic equation. Based on these studies, all results can be well understood, as shown in Eq. (9). Now we know that the bistable system driven by a high-frequency signal within the framework of vibrational resonance is only a special case. Since the nonlinear systems driven by high frequency forcing are prevalent in nature and engineering, we expect that these results are valuable and helpful to those realistic applications. We hope that our theoretical and numerical results can be generalized and will inspire further work on more complicated relevant problems.

References

[1] Strogatz S H 1994 *Nonlinear Dynamics and Chaos*: *With Applications to Physics, Biology, Chemistry, and Engineering* (Massachusetts: Perseus Books Publishing)
[2] Pikovsky A, Rosenblum M and Kurths J 2001 *Synchronization: A Universal Concept in Nonlinear Sciences* (Cambridge: Cambridge University Press)
[3] Perez R and Glass L 1982 *Phys. Lett. A* **90** 441
[4] Ding E J 1986 *Phys. Rev. A* **34** 3547
[5] Parlitz U and Lauterborn W 1987 *Phys. Rev. A* **36** 1428
[6] Rajasekar S and Lakshmanan M 1988 *Physica D* **32** 146
[7] Linsay P S 1981 *Phys. Rev. Lett.* **47** 1349
[8] Kao Y H and Wang C S 1993 *Phys. Rev. E* **48** 2514
[9] Pivka L, Zheleznyak A L and Chua L O 1994 *Inter. J. Bifur. Chaos Appl. Sci. Eng.* **4** 1743
[10] Glass L, Guevara M R and Perez A S R 1983 *Physica D* **7** 89
[11] Epstein I R and Pojman J A 1998 *An Introduction to Nonlinear Chemical Dynamics*: *Oscillations, Waves, Patterns, and Chaos, Topics in Physical Chemistry* (New York: Oxford University Press)
[12] Tai C F, Groat W C and Roppolo J R 2005 *IEEE Trans. Neural. Syst. Rehabil. Eng.* **13** 415
[13] Tai C F, Groat W C and Roppolo J R 2005 *IEEE Trans. Neural. Syst. Rehabil. Eng.* **52** 1323
[14] Bhadra N, Lahowetz E A, Foldes S T and Kilgore K L 2007 *J. Comput. Neurosci.* **22** 313
[15] Wang L Y and Kaczmarek L K 1998 *Nature* **394** 384
[16] Koblischka M R, Wei J D, Kirsch M and Hartmann U 2006 *Jpn. J. Appl. Phys.* **45** 2238
[17] Blekhman I I 2000 *Vibrational Mechanics. Nonlinear Dynamic Effects, General Approach, Applications* (Singapore: World Scientific Press)
[18] Blekhman I I 2004 *Selected Topics in Vibrational Mechanics* (Singapore: World Scientific Press)
[19] Thomsen J J 2005 *Inter. J. Bifur. Chaos* **15** 2799
[20] Thomsen J J 2008 *J. Sound Vibr.* **311** 1249
[21] Kivshar Y S, Rodelsperger P and Benner H 1994 *Phys. Rev. E* **49** 319
[22] Landa P S and McClintock P V E 2000 *J. Phys. A: Math. Gen.* **33** L433
[23] Liang R Y, Xi J, Zhao L, Zou C R and Wei C H 2012 *Acta. Phys. Sin.* **61** 134305 (in Chinese)
[24] Zhang L, Zhong S C and Peng H 2012 *Acta. Phys. Sin.* **61** 130503 (in Chinese)
[25] Wang C J 2012 *Acta. Phys. Sin.* **61** 010503 (in Chinese)
[26] Jiang L L, Luo X Q and Wu D 2012 *Chin. Phys. B* **21** 090503
[27] Yang J H and Liu X B 2010 *Chin. Phys. B* **19** 050504
[28] Ullner E, Zaikin A, García-Ojalvo J, Bascones R and Kurths J 2003 *Phys. Lett. A* **312** 348
[29] Deng B, Wang J, Wei X L, Tsang K M and Chan W L 2010 *Chaos* **20** 013113
[30] Deng B, Wang J and Wei X L 2009 *Chaos* **19** 013117
[31] Cubero D, Baltanás J P and Casado-Pascual J 2006 *Phys. Rev. E* **73** 061102
[32] Blekhman I I and Landa P S 2004 *Int. J. Non-Linear Mech.* **39** 421
[33] Casado-Pascual J and Baltanás J P 2004 *Phys. Rev. E* **69** 046108
[34] Chizhevsky V N and Giacomelli G 2006 *Phys. Rev. E* **73** 022103
[35] Chizhevsky V N and Giacomelli G 2004 *Phys. Rev. E* **70** 062101
[36] Chizhevsky V N and Giacomelli G 2005 *Phys. Rev. A* **71** 011801
[37] Khovanov I A and McClintock P V E 2007 *Phys. Rev. E* **76** 031122
[38] Yao C G and Zhan M 2010 *Phys. Rev. E* **81** 061129
[39] Yao C G, Liu Y and Zhan M 2011 *Phys. Rev. E* **83** 061122
[40] Gandhimathi V M, Rajasekar S and Kurths J 2006 *Phys. Lett. A* **360** 279
[41] Jeyakumari S, Chinnathambi V, Rajasekar S and Sanjuan M A F 2009 *Phys. Rev. E* **80** 046608
[42] Jeyakumari S, Chinnathambi V, Rajasekar S and Sanjuan M A F 2009 *Chaos* **19** 043128
[43] Zaikin A A, López L, Baltanás J P, Kurths J and Sanjuan M A F 2002 *Phys. Rev. E* **66** 011106
[44] Gandhimathi V M, Rajasekar S and Kurths J 2006 *Phys. Lett. A* **360** 279
[45] Chizhevsky V N, Smeu E and Giacomelli G 2003 *Phys. Rev. Lett.* **91** 220602
[46] Baltanás J P, López L, Blechman I I, Landa P S, Zaikin A, Kurths J and Sanjuan M A F 2003 *Phys. Rev. E* **67** 066119
[47] Hu G, Ditzinger T, Ning C Z and Haken H 1993 *Phys. Rev. Lett.* **71** 807
[48] Rappel W J and Strogatz S H 1994 *Phys. Rev. E* **50** 3249
[49] Meucci R, Gadomski W, Ciofini M and Arecchi F T 1994 *Phys. Rev. E* **49** R2528
[50] Qu Z L, Hu G, Yang G and Qin G R 1995 *Phys. Rev. Lett.* **74** 1736